CHAPTER «PHYSICAL AND MATHEMATICAL SCIENCES»

NANOSCALE METAL FILM ELECTRONICS

Roman Bihun[1]
Bohdan Koman[2]

DOI: https://doi.org/10.30525/978-9934-26-406-1-1

Abstract. The **purpose** of work is the development of technique for the deposition of nanoscale metal condensates of fine-crystalline structure of Au, Ag, Cu and transition (Mn, Hi, Pd and Cr) metals on the surface of amorphous glass or carbon substrate, and such surfaces pre-coated with wetting weakly conductive underlayers of Ge, Sb or Si, with mass thicknesses up to 8 nm. With predicted, controlled structure and electrophysical properties of metal films by use the combination of "quench deposition" technology and wetting underlayers with subsequent thermal stabilization in the interval of the first temperature zone of the modified Movchan-Demchyshyn Zone model. **Practical implication.** To analyze theoretical approaches for quantitative prediction of size charge transport phenomena in classical and ballistic regimes and the impact of surface inhomogeneities on them. Experimentally study the physical regularities of dimensional effect impact on the structure, electrophysical and optical properties of nanoscale condensates of the studied metals. The goal tasks must be **solved**: Develop a method of controlled metal films deposition with given physical parameters. Investigate fine-crystalline metal films with a given structure and establish criteria for the selection of wetting underlayers. To experimentally investigate the size dependence of the average linear sizes of crystallites *D* in the studied metal films to predict the features of the structure, surface morphology, and patterns of change in

[1] Doctor of Physical and Mathematical Sciences, Associate Professor,
Associate Professor of the Physical and Biomedical Electronics Department,
Lviv National Ivan Franko University, Ukraine
[2] Doctor of Physical and Mathematical Sciences, Professor,
Professor of the System Design Department,
Lviv National Ivan Franko University, Ukraine

the d_c percolation thickness in metal condensates. To study the regularities of condensate formation with given average linear dimensions of crystallites depending on the nature of the material, the thickness of the wetting underlayer and the mode of thermostabilization of their properties. **Methodology.** Nanoscale metal condensates (films) were depositeded with method of "frozen condensation" (quench deposition) of condensation of vapor thermally evaporated at ultra-high vacuum (pressure of residual gases did not exceed 10^{-7} Pa) of metal on an amorphous glass substrate or substrate cooled to 78-90 K, pre-covered with wetting Ge, Sb or Si underlayer of given mass thickness. The thickness of investigated films was monitired by shift of the resonant frequency of quartz vibrator. Electrical and thermoelectric power studies of the films consisted in studying of size dependence of their kinetic coefficients. Films resistance of correct geometric shape samples were measured by two-probe method, thermoelectric power with compensation method. Structure of studied films was monitored with transmission electronography and electron microscopy. The morphology of film surface was studied by scanning tunneling microscopy (STM) and atomic force microscopy (AFM). The listed approaches were performed by complementary and mutually controlled experimental and theoretical approaches. Metal films mechanical tensiones grown by thermovacuum evaporation method in VUP-5A chamber under vacuum not worse than 10^{-5} Pa were studied. Chemically polished surfaces of single-crystal silicon plates of KEF – 4.5 (111) were used for metal film mechanical tensiones investigation. Residual mechanical tensiones of the substrates caused by their mechanical processing were removed by annealing in vacuum at temperature ~ 1000°C (±1°C). After the final etching in the polishing herbator SR-4, Si-substrates were cut by dimensions of $70 \times 4 \times 0.25$ mm^3. **Practical implication.** Experimental investigation are necessary for the development of methods of controlled nanosized layers deposition of more refractory metals (in particular, Ta, Re, Hf and others), which is promising for use in modern micro- and nanoelectronic technology. **Value/ originality.** The complex technique of controlled deposition of nanoscale metal films with a predetermined structure and predicted electrophysical and optical properties in a wide range of thicknesses has been created. Metal films preparing process with specified average linear grain sizes was achieved by use the methods of "frozen condensation" and weakly conductive wetting underlayers substances that prevent coalescence of metal nuclei and selection

of temperature stabilization mode at temperatures close to the upper limit of the first temperature zone of Movchan-Demchyshyn Zone model.

1. Introduction

Metal films with thickness of several nanometers are promising as ohmic conductors with high optical transparency of electromagnetic radiation in the visible and infrared regions of the spectrum in micro-, nanoelectronics and nanoplasmonics devices. The main task of modern thin-film technologies is the development and search for methods of preparing nanoscale condensates of metals with predetermined structure and predictable electro-optical properties. The technique of films preparing in ultra-high vacuum by condensation of thermally evaporated metal on cooled substrate, ensures proper controllability of film growth process and highest purity of prepared film samples. The implementation of modern methods of film preparation is possible with the availability of the widest possible information about the peculiarities of the interaction of metal atoms between themselves and the surface of the substrate in the process of nucleation of condensate, about the mechanisms of film growth processes, which can be controlled by changing the temperature of the substrate, modifying the surface thanks to the preliminary application of surface-active substances to the surface of the substrate. In particular, it turned out that the control of the average linear size of the crystallites in the film is realized by combining the technology of "frozen condensation" (quench deposition) of a metal vapor on a cooled substrate and the preliminary application on this substrate of straining weakly conductive underlayers of the appropriate mass thickness, which inhibit the coalescence processes of the nuclei of metal crystallization phase [1, p. 121] due to origination of covalent bond with metal atoms [2, p. 996; 3, p. 12]. Electrically continuous films of metals whose structure and physical properties are stable at operating temperatures higher than room temperature are interesting for practical use in elements of micro- and nanosystem technology. The temperature stability of films structure can be judged on the basis of the temperature zones model of material films growth proposed by Movchan and Demchyshyn [4, p. 84–85] based on the generalization of the results of own experimental studies and experimental data of Palatnyk with employees [4, p. 85; 5, p. 7348]. According to the Movchan-Demchyshyn zone model, material film growth on a dielectric substrate at

temperatures $T_{sub} < 0{,}3T_{melt}$ (T_{melt} – material melting temperatures) ensures at fixed vapor condensation rate, the growth of film with average linear crystallite sizes D independent of temperature and film thickness d. As the mass thickness increases, the structure of the metal film undergoes changes from granular structure with activation mechanisms of charge transport to electrically continuous layer with metallic character of conductivity. This transition begins at some minimum d_c thickness (flow threshold), when the first metal channel with ohmic charge transport mechanism. The value of d_c can be evaluated on experimental data of size dependences of metal films DC electrical conductivity $\sigma(d)$ or films optical transmittance. Electron transport in films differs against electrical transport in bulk metal sample due to additional current carriers relaxation on film surface that are absent in bulk metal. The impact of these additional current carriers scattering on the kinetic coefficients of films is described on theories of size phenomena, which take into account the contributions of surface and grain boundary scattering of ekectrons in total relaxation time of current carriers. In addition, a significant limitation of the linear dimensions of the sample can lead to changes in its electronic structure and thus affect kinetic phenomena. There are a number of approaches for quantitative prediction of kinetic properties of films depending on layer thickness, linear dimensions of crystallites, and parameters of surface inhomogeneities, the right choice of which will allow reliable prediction and quantitative description of kinetic coefficients of nanoscale metal films in a wide range of thicknesses.

The purpose of work is devoted to considering the principles of creating techniques for the controlled preparation of films of base and transition metals with a given structure (controlled average linear dimensions of crystallites), mechanical properties, surface morphology, predictable electrical and optical properties, based on combination of "frozen condensation" (quench deposition) method, the use of wetting weakly conductive layers, which weaken the effect of nuclei coalescence phenomenon of metal phase crystallization, and thermal stabilization of layer within the first temperature zone of the modified Movchan-Demchyshyn Zone approach. The obtained results are necessary for the use and further development of controlled methods of deposition of nanoscale condensates of more refractory metals (in particular, Ta, Re, Hf and others), which are promising in modern micro- and nanoelectronic technology.

2. Metal films growth on the surface of amorphous substrate

The deposition of metal film on the substrate surface is characterized by the process of surface adsorption and the appearance of nuclei crystallization. Germ growth is observed at high supersaturation of condensate steam $S = P / P_0$(1), where P – vapor pressure of deposited metal evaporated from the source at temperature T_{evap}, P_0 – the equilibrium vapor pressure of the material at the surface of the substrate at the temperature of the substrate T_{sub}. In the process of condensation of a single-component vapor, there is monomolecular and dissociative adsorption, which at small numbers of filling degrees of the substrate lead to the uniform appearance of adatoms on the incompletely occupied surface of the substrate at a constant rate [1, p. 102]. The deposition rate R is a function of vapor pressure of the deposited metal $R = C_g \sqrt{2\pi m k_B T_{avap}}$ (2), where C_g – geometric parameter, k_B is the Boltzmann constant, m is the molecular weight of the deposited metal, and T_{avap} is the temperature of the evaporation source. Supersaturation S is large parameter: $S = 10^5$-10^{50} ($S > 4$ in Wilson's chamber), therefore, the nucleation process is a non-equilibrium process that can be well described within mean field nucleation theory [2, p. 486].

After the adsorption of metal atoms on the surface of the amorphous substrate, the formation of nuclei and islands is observed, which increase in size and concentration as the mass thickness of the metal film increases. The gaps between the islets decrease, with the subsequent process of islet coalescence and the growth of larger clusters. The observed process is illustrated by the experimental data of the work [1, p. 38–50; 3, p. 6] (Figure 1). The successive increase in the mass of the condensed layer allows the formation of structures whose electrical properties change continuously. Note the existence of a critical thickness of the dc metal layer at which the metal islands form the first continuous channel with metallic conductivity (a cluster of infinite dimensions).

Depending on atoms interaction on substrate with the atoms of the film, three modes of film growth are distinguished (Figure 2). Island mode (**Volmer-Weber mode** (Figure 2(a)), in this mode, clusters originate directly on the surface of the substrate, subsequently forming island phases of the condensate. This growth regime is characteristic of many condensates, including metals deposited on substrates of amorphous metals, graphite or mica. In the layer-on-layer mode (**Frank–van der Merwe mode**

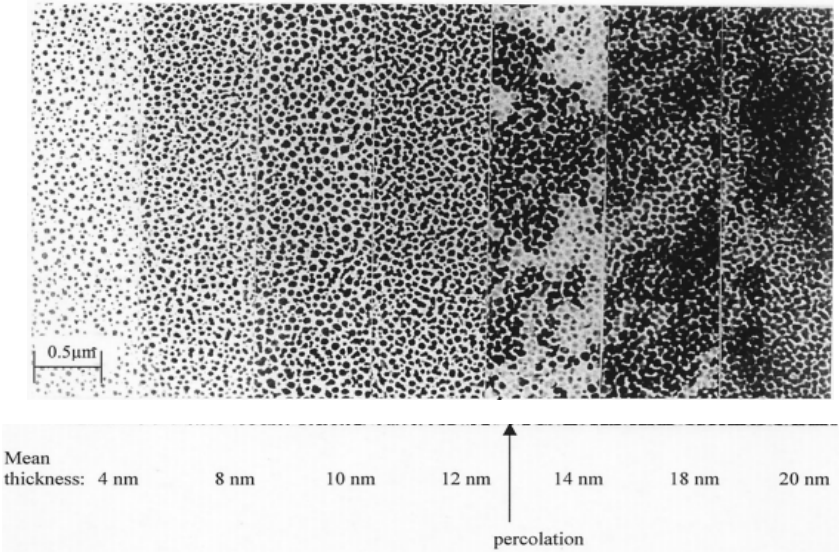

Figure 1. Electron microscopy of evolution of antimony Bi films of different thicknesses growth (nucleation, nuclei growth, coalescence, channels, cavities, homogeneous film)

(Figure 2(c)), the situation is opposite due to the fact that condensate atoms interact more strongly with the substrate than with each other. The first atoms during condensation on the surface of the substrate form a solid monolayer, which is later covered by a second layer of condensate, the binding energy of the newly formed layer is lower compared to the first monolayer. This mode corresponds to the layer-by-layer growth of metal condensate on the surface of the substrate. This regime is characteristic of adsorbed gases, in particular, when an inert gas is adsorbed on the surface of carbon or a metal substrate, as well as for some "metal-metal" systems, and when semiconductor condensate forms on the surface of a semiconductor. The mixed mode (**Stranski–Krastanov mode** Figure 2(b)) is a rather interesting intermediate case. Where after the formation of the first monolayer (ML) or several monolayers, further layer-by-layer growth becomes thermodynamically disadvantageous. As a result, islands begin to grow on the surface of the "intermediate layer". There are many different

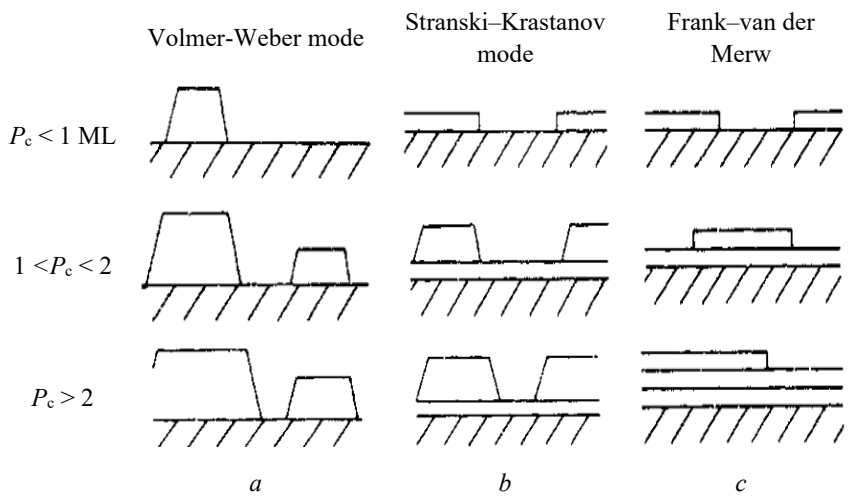

Figure 2. Schematic representation of three modes crystallite growth: (a) Island mode or Vollmer-Weber mode, (b) layer plus islands mode or Stransky-Krastanov mode, (c) layer by layer or Frank van der Merwee mode. P_c – monolayers fill facto r(ML)

reasons for this formation, so any factor that disrupts the monotonous decrease in bond energy between layers can be the cause of this behavior.

For most metal films, the percolation thickness d_c varies in the range of 1-20 nm depending on a number of factors. At the mode of metal continuous deposition on the substrate surface the thermodynamic regime can change depending on four processes: Shading, Surface Diffusion, Volume Diffusion and Recrystallization. For most metals and dielectrics the diffusion activation energy depends on material melting temperature of condensate T_{melt}. At different substrate temperature ranges, one should expect one or another regime to prevail. This problem was first noticed by Movchan and Demchyshyn [4, p. 83–89; 5, p. 7350; 6, p. 654] in metal films with thickness of 100 nm. According to [4; 6], the process of condensate restructuring on the surface of the dielectric substrate can be influenced through temperature zones (Figure 3):

1. The first temperature zone $T_{sub} < 0{,}3T_{melt}$ (characterized by low mobility of atoms, adatoms stick to the place of landing on the surface of

the substrate, resulting in the formation of a fine-crystalline, porous film of condensate).

2. The second temperature zone $0{,}3T_{melt} < T_{sub} < 0{,}5T_{melt}$ (surface diffusion occurs at an activation energy of 0,1-0,3 eV, a columnar growth of the condensate film is observed).

3. The third temperature zone $T_{sub} > 0{,}5T_{melt}$ (at activation energy greater than 0,3 eV the bulk diffusion occurs); a film of large uniaxial crystallites is growed.

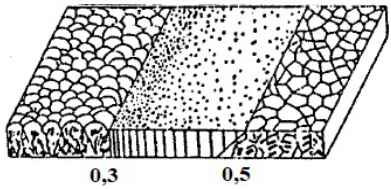

Figure 3. Temperature zones of film condensate formation [4–6]

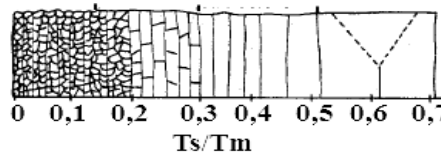

Figure 4. Structural zones according to Grovenor [7]

Later, the model of temperature zones was refined. In particular, in [5], when the structure of thin gold films deposited on a dielectric substrate was studied, four temperature zones were distinguished. At a low temperature of the substrate Tpid, which met the criterion $T_{sub} < 0{,}1T_{mel}$, a mode of sharply cooled condensation ("quench deposited") was observed (Figure 4). The "quench deposited" mode is used for fundamental research on the problems of superconductivity, localization, and quantum phase transfer. One of the disadvantages of "quench deposited" is the occurrence of metastable states, which strongly affect the kinetic phenomena in metal condensates. However, X-ray and electron microscopic studies of "quench deposited" Au, Cu, Ag, Pb and Cs films with a thickness greater than 10 nm indicate their stable, polycrystalline structure [5]. The critical thickness of metal film polycrystalline structure strongly depends on the nature of material and can vary in a wide range of thicknesses. Therefore, the films structural studies of investigated metals were carried out in order to get information about the correspondence of the crystal lattice parameters of metal condensates with the crystal lattice parameters of massive metals, their homogeneity and isotropicity, and as well as the state of condensates

surface morphology. Electronographic study of deposited films structure at $T = 78$ K on amorphous carbon surface and thermally stabilized at temperatures of 300 K or 370 K showed that the metal films structure are homogeneous and polycrystalline without predominant crystallite orientation. No impurity or non-equilibrium phases were detected in the metal films deposited on the surface of wetting underlayers. On Figure 5 we shows electron diffractograms picture of Cr, Ni, Au and Cu metal films with thickness 20 nm. We can see that Cr films are polycrystalline layers with cubic body-centered crystal lattice, unlike Ni, Au, and Cu films, which have a face-centered cubic lattice. The calculated parameters of the elementary cells are within the accuracy of the experiment (the accuracy of calculated parameters of the crystal lattice is no worse than 0,001 nm), similar to the parameters of crystal lattice of bulk metals. Among other studies the metal films structure, films continuity and average linear dimensions D of films crystallites of different mass thicknesses and parameters of surface inhomogeneities in macroscopic scale were studied. Based on analysis of experimental data of film structure examination with STM and transmission electron microscopy, the information about the continuity and uniformity of metal condensate structure was obtained. It was shown that metal films are homogeneous and continuous polycrystalline samples in the post-percolation range of thicknesses, which is also consistent with the predictions of percolation model [7, p. 91–93]. For films of the studied metals deposited on a clean amorphous surface, this is manifested at least up to a thickness of about 12-15 nm. Metal films deposited on the surface of wetting weakly conductive underlayers (Ge, Si, Sb) are continuous at smaller thicknesses

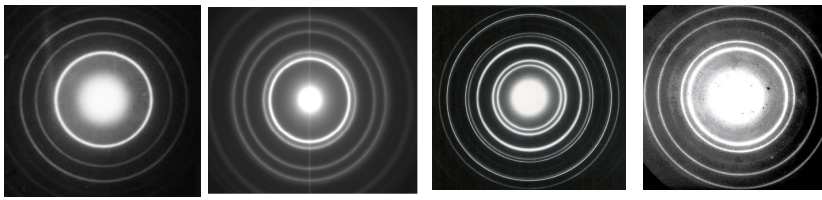

a) chrome b) nickel c) gold d) copper

Figure 5. Electron patterns of chromium (a), nickel (b), gold (c) and copper (d) films with a thickness of 20 nm deposited on an amorphous carbon film (20 nm)

(depending on the mass thickness of the wetting underlayers) due to a decrease in the average linear dimensions of the crystallites and an increase in the density of metal filling of the surface of the substrate. In Figure 6 shows electron *D* in a light microphotograph of gold films with a bulk thickness of 2 nm formed on a pure amorphous substrate (Figure 6 a) and on an amorphous substrate pre-coated with germanium underlayers with bulk thicknesses of 2 nm (Figure 6 b) and 3 nm (Figure 6 c). As a result of the analysis of the histograms of the linear sizes of the crystallites in the films (Figure 7), it is shown that the influence of the germanium underlayers is reduced to a decrease in the crystallite sizes.

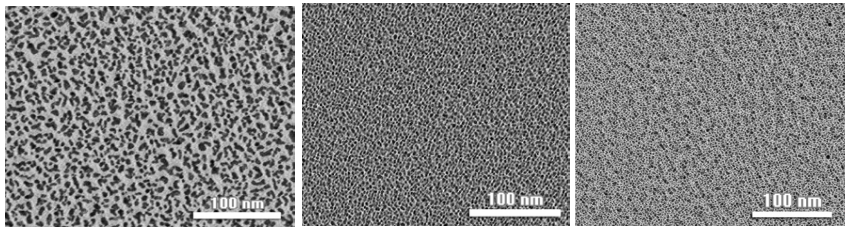

(a) Au 2 nm (b) Au 2 nm, Ge 2nm (c) Au 2 nm, Ge 3nm

Figure 6. Microstructure of Au films with mass thickness of 2 nm deposited on clean carbon substrate (a) and on a carbon substrate previously covered with Ge wetting underlayers with a mass thickness of 2 nm (b) and 3 nm (c)

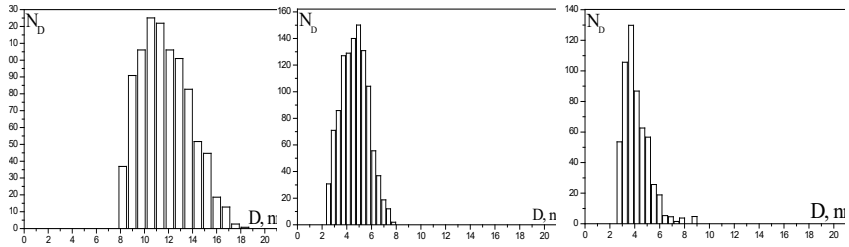

(a) (b) (c)

Figure 7. Histograms of crystallite size distribution on the surface of substrate covered with Au films with a mass thickness of 2 nm, deposited on a pure carbon substrate (a) and on carbon substrate pre-coated with Ge wetting underlayers with mass thickness 2 nm (b) and 3 nm (c)

This is evidenced by the shift of the maxima of the corresponding distributions to the area of smaller thicknesses. At the same time, the homogeneity of the metal condensate layer is increased (the decreas of distributions the half-width of histograms, Figure 7). After analysis of size dependences metal film filling factor P with metal condensate (Figure 8), it can be seen that the germanium underlayers contribute to a more uniform and high filling density of substrate surface with metal clasters. That counteracting the metal clusters coalescence and contributes to the layer-by-layer growth of metal condensate on the surface of the substrate.

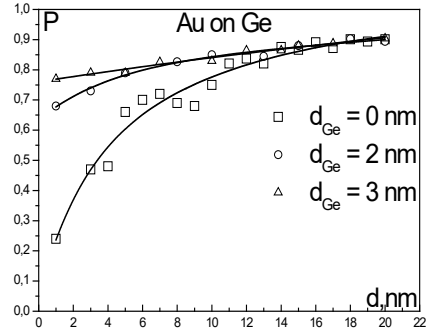

Figure 8. Size dependences of the metal film filling factor with Au films deposited on amorphous (a) and pre-coated substrate with Ge wetting underlayers with mass thicknesses of 2 nm (b) and 3 nm (c)

We examine the impact of Ge, Si and Sb wetting underlayers on metal films crystallites average linear sizes *D* in all studied metals. A key feature

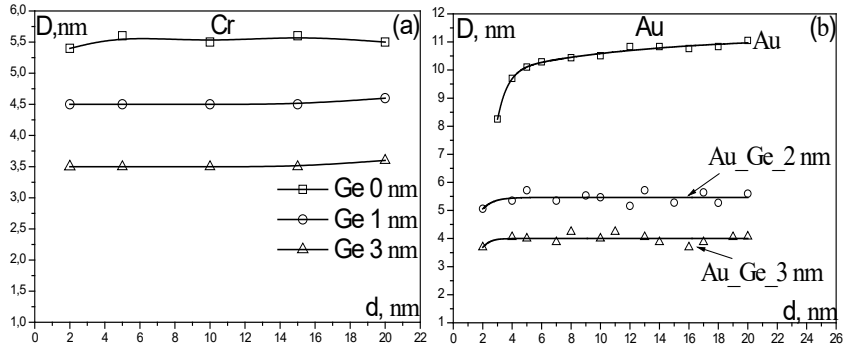

Figure 9. Size dependences of the crystallites average linear sizes in Cr (a) and Au (b) films of different thicknesses deposited on pure amorphous substrate and on substrate pre-coated with germanium underlayers of different mass thickness up to 3 nm

of investigated metal film deposition on the surface of wetting underlayers is the invariance of the crystallites average linear sizes D while increasing the condensate thickness, in the studied size range of metal film thicknesses (Figure 9).

4. The impact of size effect on charge transport in nanoscale metal films

The problem of the difference between the electrical conductivity of metal film and conductivity of bulk metal was first considered in the works of Thomson (1901) and Lovell (1936) [8, p. 101; 9, p. 224]. They were based on the assumption of geometric effect (size effct), which consisted in limiting the electron mean free path length λ_e by the surfaces of film. According to Sommerfeld metal model, there is a relationship between the specific conductivity σ_0 and the free path length λ_0 of current carriers in a bulk metal sample, based on which the concentration n of free current carriers can be evalueted: $\frac{\sigma_0}{\lambda_0} = \frac{ne^2}{m\langle v\rangle} = \left(\frac{8\pi}{3}\right)^{1/3} \frac{e^2 n^{2/3}}{2\pi\hbar} = 7{,}1\times10^7 n^{2/3}$, where e – electron charge, $\hbar$ – Planck's reduced constant. The first consistent approach for describing the impact of surface scattering effect on carriers charge transport in film were developed by Fuchs [8, p. 101] and Sondheimer [10, p. 522]. Considering a plane-parallel metal sample with a Sommerfeld gas of free electrons, Fuchs [8, p. 102] applied the Boltzmann kinetic equation with the appropriate boundary conditions, which took into account the influence of the size effect, and calculated the size dependence of the specific conductivity of the metal film $\sigma(d)$. The result of Boltzmann kinetic equation integration for single-layer, plane-parallel metal film is given by Sondheimer function [8, p. 103; 10, p. 523]:

$$\Omega(k) = \rho_\infty / \rho = \sigma_\infty / \sigma_0 = 1 - \frac{3(1-p)}{2k} \int_1^\infty \left(\frac{1}{t^3} - \frac{1}{t^5}\right) \cdot \frac{1-e^{-kt}}{1-pe^{-kt}}\, dt, \quad (1)$$

where σ_∞ and ρ_∞ – conductivity and resistivity of thin film infinite thickness ($d \to \infty$), which structure is identical to the structure of investigated film, $k = d/\lambda$ – normalized thickness, λ – electrons mean free path. The Sondheimer function makes it possible to evaluate the size dependence of resistivity $\rho(d)$ or conductivity $\sigma(d)$ of electrically continuous metal film, the structure of which is identical to the structure of the investigated film.

It should be noted that in the approximation of the classical size effect [10, p. 523] it is assumed that the electronic structure of metal is similar to the structure of bulk sample. Fuchs-Sondheimer approach proved to be very useful in the interpretation of experimental data in approximation $d >> \lambda$. Within the framework of the classical size effect, size dependences of thin metal films kinetic coefficients were calculated: the temperature coefficient of resistance β, the Hall constant R, and the absolute differential thermoelectric power S [10, p. 535–538]:

$$\beta / \beta_{\infty} = F(k), \; R / R_{\infty} = F(k) / \Omega(k), \; S / S_{\infty} = [1 + UF(k)] / (1 + U), \quad (2)$$

where $F(k) = 1 - [k / \Omega(k)] \partial \Omega(k) / \partial k$, $U = 2$ (free electron model), β_{∞}, R_{∞}, S_{∞} – corresponding kinetic coefficients of infinite thickness film ($d \to \infty$). Based on analysis of size dependences of thin metal films kinetic coefficients (2), it can be seen that the size effect is strongly manifested in resistivity $\rho(d)$ and temperature coefficient of resistivity $\beta(d)$ (Figure 10), weakly in Hall constant R. Therefore, when studying the electron transport properties of films in the range of thicknesses ($d \geq \lambda$), size effect in R are not taken into account. In practice, when calculating kinetic coefficients, the asymptotic approximations of expression (1) are considered in two regions:

$\lambda << d$ (3) :

$$\rho / \rho_{\infty} = \sigma_{\infty} / \sigma = 1 + 0{,}375 \lambda (1 - p) / d,$$
$$\beta / \beta_{\infty} = 1 - 0{,}375 \lambda (1 - p) / d,$$
$$R \approx R_{\infty},$$
$$S / S_{\infty} = 1 - 0{,}375 \lambda (1 - p) U / [d(1 - U)].$$

$\lambda >> d$ (4):

$$\rho/\rho_{\infty} = \sigma_{\infty}/\sigma = 4\lambda(1\text{-}p)/[3d(1+2p)\ln(\lambda/d)]$$
$$\beta/\beta_{\infty} = \ln(\lambda/d),$$
$$R/R_{\infty} = 4\lambda(1\text{-}p)/[3d(1+2p)\ln^2(\lambda/d)],$$
$$S/S_{\infty} = \{1+U[\ln(d/\lambda)\text{-}1{,}42]\}/[(1+U)[\ln(d/\lambda)\text{-}0{,}42])].$$

For $d \geq (0{,}1 - 0{,}2)\lambda$, the equations (3) with accuracy no worse than 5% describes the size experimental dependences of kinetic coefficients of thin metal films. The analysis of the size dependence of the combined resistivity coefficient (Figure 10) also indicates the fact that in the case of fully specular scattering ($p = 1$) the dimensional effect in the change of the resistivity $\rho(d)$ is not manifested, except in the case of an increase in the contribution of surface scattering ($p = 0$), the dimensional effect is manifested for a wider range of metal film thicknesses. The analysis of the behavior of the size dependences of the kinetic coefficients (3) – (4) is detail discussed in [10–18, p. 532]. The size-dependent surface scattering is the cause of the

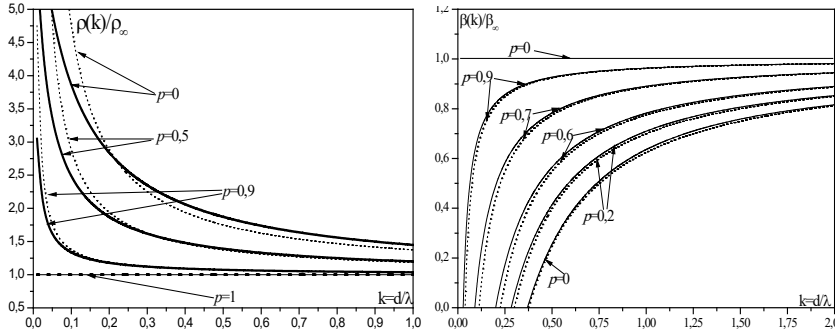

a) b)

Figure 10. Kinetic coefficients size dependences of resistivity $\rho/\rho_\infty = f(k)$ (a) and temperature coefficient of resistivity $\beta/\beta_\infty = f(k)$ (b) on $k = d / \lambda$, p – specularity paramiter of the surface dispersion of current carriers ($0 < p < 1$). Solid curves are theoretical expressions of Sondheimer function, non-solid curves are asymptotic expressions of the Fuchs-Sondheimer approach in approximation of thick films (3)

size effect in the electrical conductivity of metal films. To describe surface scattering, we introduce the concept of residual conductivity σ_{res}, which is a physical characteristic of the dimensional effect of surface scattering: $\sigma_{res} = 1/[\rho(d) - \rho_\infty]$. Analysis of dimensional progress of residual conductivity σ_{res}, shows $\rho_\infty\sigma_{res} = 8d/[3\lambda(1-p)] \sim d$. Appropriate presentation $\rho_\infty\sigma_{res}$ according to the data on Figure 10 (a) is presented in Figure 11. Analysis of dimensional dependencies $\rho_\infty\sigma_{res} = \rho_\infty\sigma_{res}(k)$ indicates that the change in the coefficient of surface specularity p has little effect on the variation in value $\rho_\infty\sigma_{res}$, while, the slope of the curve (an indicator of the power of the metal film thickness) remains unchanged and close to unity in a wide range of film thicknesses ($k > 0{,}1$).

Mayadas and Shatzkes (MS) [19, p. 345–446; 20, p. 1383] made an attempt to describe the contribution of crystal boundary to the total scattering of electrons in polycrystalline films of brooms. It is assumed that the film consists of one layer of crystallites of equal size with contacting boundaries between them, perpendicular to the external parallel planes that limit the film (Figure 12 a). To describe the grain boundary, the potential –

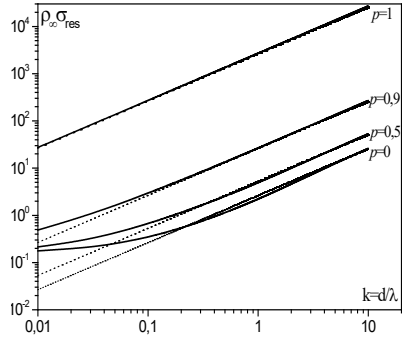

Figure 11. Size dependencies of $\rho_\infty\sigma_{res} = \rho_\infty\sigma_{res}(k)$ for different coefficient *p*. Solid curves – Sondheimer theoretical expressions (1), non-solid curves – Fuchs-Sondheimer approximation

function is introduced, and it is assumed that electron scattering occurs only on boundaries perpendicular to the electric field vector. Grain-boundary scattering occurs simultaneously with bulk scattering and independently of it (Mathiessen's law). Mayadas and Shatzkes [19, p. 447; 20, p. 1385] have got the relation of polycrystalline film resistivity:

$$\frac{1}{\rho(d)} = \frac{1}{\rho_g} - \frac{6(1-p)}{\pi k \rho_0}\int_0^{\pi/2} d\Phi \int_0^{\infty} dt\, \frac{\cos^2\Phi}{H^2(t,\Phi)}\left(t^3 - t^2\right)\frac{1-\exp\left(-\left[ktH(t,\Phi)\right]^{-1}\right)}{1-p\exp\left(-\left[ktH(t,\Phi)\right]^{-1}\right)}, \quad (5)$$

where $H(t,\Phi) = 1 + \alpha \Big/ \left(\cos\Phi\sqrt{1-t^2}\right)$, $a = \lambda_0 r / D(1-r)$ – structure paramiter, D – average linear crystallite diameter; r – grain boundary scattering coefficient at the crystallite interphase boundary, which depends on the nature of the boundary and the presence of impurities on it ($0 \le r \le 1$); λ_0 – electron mean free path in a single crystal; ρ_0 та ρ_g – resistivitity of monocrystalline and polycrystalline (phonons, point defects, and grain boundaries) massive samples, respectively; Φ – the angle of electron incidence to the grain boundary. In the limiting case of rough films ($d >> \lambda$): $\sigma_\infty / \sigma_0 = \rho_0 / \rho_\infty \approx f(\alpha)$, $f(\alpha) = 1 - 1{,}5\alpha + 3\alpha^2 - 3\alpha^3 \ln(1 + 1/\alpha)$ – Mayadas and Shatzkes function (Figure 12 *c*).

Tellier, Tosser and Pichard (TTP) [21, p. 310–316; 22–30] calculated the parameters of electrical transfer in polycrystalline films under the assumption

that the crystallites grow in the form of cubes that are closely adjacent to each other (Figure 12 b). In [30, p. 62], a model of effective electron free path was developed and in [21, p. 123] – an isotropic scattering model.

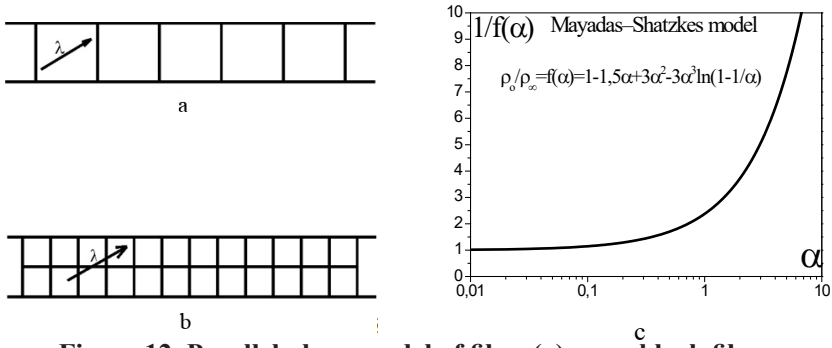

Figure 12. Parallel plane model of film: (a) monoblock film; (b) fine crystaline film and (c) Mayadas-Shatzkes function 1 / *f* (α)

Within the framework of the TTP approach, the absence of temperature [23, p. 219] and energy dependence [24, p. 868] of the grain boundary scattering coefficient t was discovered. The deviation of the real shape of the crystallites in the film from the cubic shape was theoretically analyzed in [25, p. 811]. It is shown that the shape of the crystallites (cubic-spherical) slightly changes the longitudinal kinetic effects (conductivity, temperature coefficient of resistivity and thermal-t.e.f), and the value of *t* does not depend on the crystallite shape. Expressions for electrical conductivity of metal films with shape-changing texture were developed in [31, p. 62; 32; 33]. Within the limits of the listed models of the internal size effect, a number of expressions for evaluting the kinetic coefficients of the experimental results were obtained. To do this, after measuring the corresponding kinetic coefficient $\rho(d)$ or $\sigma(d)$, the film thickness *d*, the average linear grain size *D*, the dimensional dependence is approximated by the corresponding approximate expression, where the fitting parameters are: the surface scattering specularity parameter *p*, the grain boundary scattering coefficient *r* or *t* – the probability of grain boundary tunneling (for theoretical of TTP approaches [26, p. 4–6]) and the average free path length of current carriers in a massive crystal. However, as noted in [10, p. 529], the approximation expressions of the Mayadas-Shatzkes (MS)

and Tellier-Tosser-Pichard (TTP) theories correctly describe the properties of solid polycrystalline films of relatively large thickness ($d \geq \lambda$), in the region of small thicknesses ($d \leq \lambda$), these approaches do not work and give physically incorrect numerical prediction of size dependencies of thin metal films kinetic coefficients.

Namba [32, p. 1326] considered structure of metal film with one-dimensional surface inhomogeneities of thickness distributed in the direction of current flow according to the harmonic law. The local thickness of the film $d(x)$ in the direction of current flow is given by the expression $d(x) = d_{cep} + h\sin(2\pi x / L)$ (6) (Figure 13), where d_{cep} – average film thickness; h – parameter of film thickness inhomogeneities (it means the average amplitude of the deviation of film thickness to d_{cep}); L – the recurrence period of macroscopic inhomogeneities of thickness in the direction of OX. The average value of size film resistivity can be calculated with expression: $\frac{\rho}{\rho_\infty} = \frac{d_{cep}}{L}\int_0^L \frac{\rho(d(x))}{d(x)}dx$ (7), where ρ_∞ – resistivity of infinite thick film, $\rho = \rho(d(x))$ – local film resistivity with thickness $d = d(x)$.

Comparison of experimental data with (7) is carried out by searching for h, which acts as the desired parameter. The dependence $\rho = \rho(d)$, is calculated with (7) for large thicknesses ($d >> h$) coincides with the Fuchs-Sondheimer prediction. At $d \approx \lambda$ this dependence goes to zero faster than predicted by Fuchs-Sondheimer theory and at $d < h$, it is $\rho \to \infty$, which corresponds to a discontinuous metal film. The ohmic mechanism of charge transport in a metal film occurs at a certain thickness $d_|$ (where $\beta > 0$), it's mean transition to electrically continuous metal films. Approximation for large thicknesses ($\lambda << d$) is expression (7):

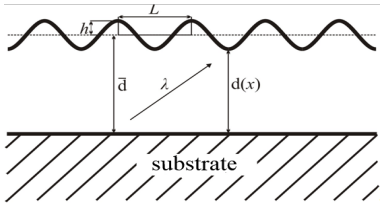

Figure 13. Namba's metal film model

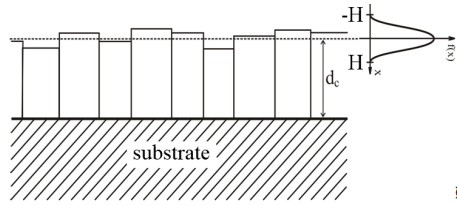

Figure 14. Wissman's metal film model

$\rho(d) = \rho_\infty \left[1 - \left(\frac{h}{d}\right)^2\right]^{-\frac{1}{2}} \left[1 + \frac{3\lambda(1-p)}{8d}\left[1 - \left(\frac{h}{d}\right)^2\right]^{-1}\right]$ (8). Expression (8) at limit $h << d$ transforms into the expression known in Fuchs-Sondheimer [10, p. 525] model for the resistivity in the limit of large thicknesses (3).

Wissman [34, p. 6–7; 35, p. 3–10] believed that total metal film resistivity is the sum of three sources of electron scattering: scattering on volume inhomogeneities, scattering on crystallite boundaries and scattering on surface inhomogeneities. Wissman [35, p. 2–3] assumed that the boundaries of the crystallites are perpendicular to the surface of the film (Figure 14). The starting point of the model is the assumption of a symmetrical distribution of the average linear sizes of the film crystallites around the average value of the film thickness (Figure 14). The average value of the specific resistance of the metal film is calculated from the ratio: $\langle\rho\rangle = \frac{\int \rho(x) f(x) dx}{\int f(x) dx}$ (9), where x – is deviation of the film thickness from average thickness *d*, $f(x)$ – surface roughness distribution function (Figure 14). A typical example is the quasi-Gaussian distribution (with full width $2H_{\max}$, Figure 14). Integration is carried out in range $-H_{\max}$ to $H_{\max}$. The value of $H_{\max}$ is numerically equal to the maximum deviation of the surface heterogeneity from the metal film average thickness d_c. Out equations (3) in case of diffuse ekectron scattering on film surface ($p = 0$), we get:

$$\rho(d,\lambda,H) = \int_{-H}^{+H} \left(1 + \frac{3}{8}\frac{\lambda}{d-x}\right) f(x) dx \Big/ \int_{-H}^{+H} f(x) dx$$

, whence

$$\rho(d,\lambda,H) = \rho_\infty + \frac{3}{8}\frac{\lambda}{d}\rho_\infty + \frac{3}{8}\frac{\lambda}{d}\rho_\infty \int_{-H}^{+H} \frac{x/d}{1-x/d} f(x) dx \Big/ \int_{-H}^{+H} f(x) dx . \quad (10)$$

At approx ($H < d$),expression $1/(1-x/d)$ can be expanded into Taylor series, whence, $\rho_r = \frac{3}{8}\frac{\lambda}{d}\rho_\infty \left(\frac{H^2}{d^2}G_2 + \frac{H^4}{d^4}G_4 + ...\right)$, де $G_n = \int_{-1}^{+1} x^n f(x) dx \Big/ \int_{-1}^{+1} f(x) dx$, ρ_r is paramiter mean resistivity due to scattering on surface inhomogeneities with maximum amplitude $H_{\max}$. Numerical values of coefficients G_2, G_4, та G_n, can be calculated

only if there is information about the real profile function of surface inhomogeneities. If we assume symmetric quasi-Gaussian distribution of surface inhomogeneities, then the coefficients: $G_2 = G_4 = G_n = 1$, then Wissman's expression [34, p. 6]:

$$\rho(d,\lambda,H) = \rho_\infty \left(1 + \frac{3}{8}\frac{\lambda}{d}\left[1 + \left(\frac{H}{d}\right)^2 + \left(\frac{H}{d}\right)^4 + \left(\frac{H}{d}\right)^6 + \left(\frac{H}{d}\right)^8 + \ldots \right] \right) \quad (11).$$

For the practical use of metal films as elements of microelectronics, it is important to know at what minimum thickness the film can be considered as electrically continuous layer with metallic conductivity. The answer to this question can be reached out of metal film resistance size dependence analys with percolation theory [36, p. 89–90]. According it, size dependence of metal film resistance can be represented by power-law: $R(d) \sim (d - d_c)^{-\gamma}$. At layer-by-layer regime of metal film growth, it is considered $(d - d_c) \sim (P - P_c)$ [36. p. 91], where P_c – the percolation parameter, which corresponds to the degree of filling of the substrate surface, at which the islands form the first conductive channel. The exponent γ depends on the mode of metal film growth mode. With film layer-by-layer growth (2D mode), the value of exponent γ change in the range $1 \le \gamma \le 1{,}3$, and for 3D percolation, the value exceeds the value of $\gamma \ge 1{,}5$. It is illustrated on Figure 15, which shows the $R = R(d)$ dependencies of Cr films freshly deposited on glass surface (curve 1) and on a glass surface pre-coated with a Ge wetting underlayer with a thickness of 8 nm (curve 2). The inset shows linearized dependencies is presented in logarithmic scale $R = R(d - d_c)$. We can see that due to the presents of Ge underlayer, percolation thickness d_c in Cr films reduced from 2 nm (Cr film on glass) to 1,1 nm (Cr film on the surface of the Ge underlayer).

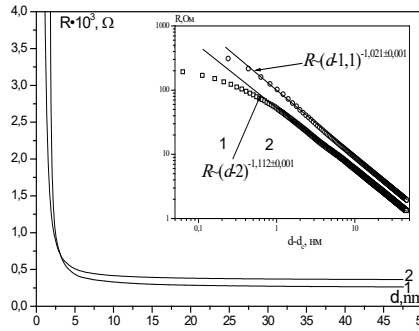

Figure 15. Size dependencies of *R*(*d*) of Cr films. 1 – chromium films deposited on a clean glass substrate; 2 – chromium films deposited on the surface of the Ge wetting underlayer with a mass thickness of 8 nm

The γ exponents are 1,112 to 1,021 respectively. It should be noted that the method of film preparation used in the work provided layer-by-layer growth of films of all studied metals with a value of $\gamma < 1{,}3$. In [37, p. 724; 38–39], the impact peculiarities of Sb and Si wetting underlayers on the *D* crystallites average size and the d_c for metal films were analyzed. Based on the data of microstructure study and the study of percolation phenomena of investigated metals films, it was shown that metal films can be considered electrically continuous metal layers with thicknesses greater than $d_{mean} = 2d_c$. The description of charge transport phenomena in metal films can be carried out with the help of quasi-classical and ballistic size effect theories [40, p. 341].

Expressions (2) – (3) are linearized when written as a dependence $\rho(d)d = f_1(d)$, $\beta(d)d = f_2(d)$ and $S(d)d = f_3(d)$. In Figure 16 shows the size dependence of gold films kinetic coefficients in low-temperature range 78 K-90 K and Figure 8 – corresponding linearized dependencies are presented. On Figure 17 shows that in the range of large thicknesses ($d > 15$ nm) size dependences $f_1(d)$, $f_2(d)$ and $f_3(d)$ are linear. In the range of small thicknesses ($d < \lambda$) the linearity is violated, which is due to the deviation of the the real film structure from plane-parallel layer model [32; 34; 40, p. 342].

Out of slope of the linear sections, we get the numerical values of ρ_∞, β_∞ and $S_\circ$. Segments cut off on the abscissa axis by the continuation of linear segments, with accuracy up to a factor of $3(1-p_e)/8$, are equal to electron mean free path ($p_e = 0$ [40, p. 352]). Such conclusion follows out the fact that the real metal surface consists of randomly placed crystallites, makes it impossible electron wave coherently reflection. Qualitatively similar dependences are obtained for freshly applied and thermally stabilized films of all metals [37, p. 730]. Note that the resistivity ρ_∞ of thermo stabilized films is lower than the resistivity of freshly deposited films and the temperature coefficient of resistance β_∞ and electrom mean free path λ have larger values compared to the corresponding characteristics of freshly depositer films (quench condensed). Since there are no visible structural changes during thermostabilization, the cause of this phenomenon is the point defects annealing present in the freshly deposited layer in the volume and on the surface of the crystallites [38, p. 534]. In [39, p. 604] the films charge transport parameters were calculated and the temperature and grain size dependencies of *t* parameter were studied. The theoretical prediction

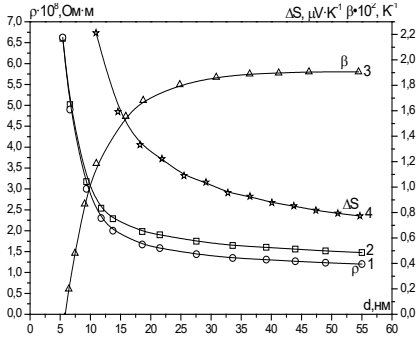

Figure 16. Size dependences of Au films kinetic coefficients on glass surface: 1 – ρ(*d*) at T = 78 K; 2 – ρ(*d*) at T = 90 K; 3 – β(*d*) and 4 – Δ*S*(*d*) at temperature range 78–90 K

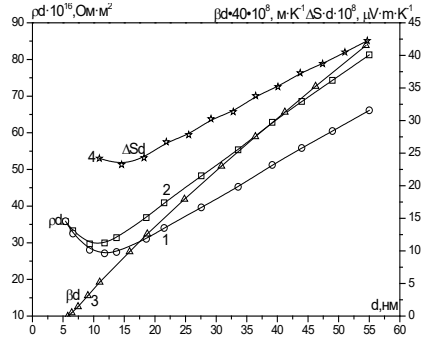

Figure 17. ρ(*d*)*d* = $f_1(d)$ size depen-dencies of Au films on the glass surface: 1 – T = 78 K, 2 – T = 90 K, 3 – β(*d*)*d* = $f_2(d)$ and 4 – *S*(*d*)*d* = $f_3(d)$ at temperature range 78–90 K

[40, p. 352] of temperature independency of t parameter (at least for the temperature range 78 K – 370 K) and grain size (5 nm $\leq D \leq$ 28 nm) was revealed. The results of the study of thermoelectric power films of metals (Au and Cu) are interpreted within the framework of free electron model. It was shown that the free electron model sufficiently reliably describes the thermo-e.r.s. films of these metals. In particular, the value of the parameter U, calculated out of our results obtained by us, turned out to be close to the value $U = 2$ ($U = 2{,}1 - 2{,}2$ for Au films, $U = 2{,}0 - 2{,}1$ for Cu films). The study of thermoelectric power of Ni and Pd films deposited on the clean glass surface and on the surface of wetting underlayers of different mass thickness is explained on model that assumes the existence in these metals of current carriers of two independent groups with different effective masses that are on electron and hole trajectories, respectively [41, p. 128; 42, p. 139]. The Fermi surface in polyvalent metals has a complex shape and in its appearance is far from the spherical shape that is the basis of the free electron model [14, p. 1083]. On the Fermi surface of the mentioned metals, there are both electronic and hole states, which determines a number of peculiarities of the behavior of charge transfer phenomena in

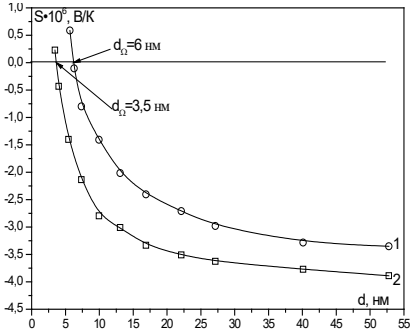

Figure 18. Size dependences of thermo-e.p.f. S of palladium films relative to platinum deposited on fused polished glass (1) and glass covered with a germanium underlayer with thickness of 0,5 nm (2)

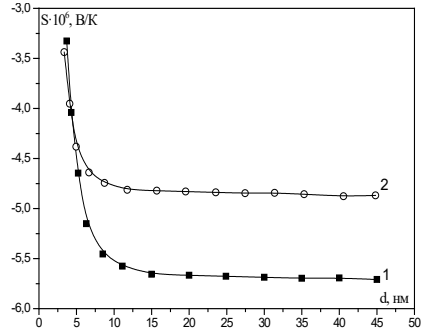

Figure 19. Size dependences of the differential thermo-e.p.f. S of nickel films relative to platinum deposited on glass (1) and on germanium underlayer with thickness of 0,5 nm (2)

films of transition metals. In films of palladium and nickel, size dependence of thermoelectric power is significantly stronger than the dimensional dependence of thermoelectric power films of base metals. Thermoelectric power of palladium films, as can be seen on Figure 18 changes its sign in films deposited on glass at a thickness of about 6 nm, and on germanium wetting underlayers at 3,5 nm.

A similar sign change of thermoelectric power of palladium films was observed in [42, p. 136]. Under the free electron model, it is impossible to explain the observed behavior. Size dependences of conductivity $\sigma(d)$ and differential thermoelectric power $S(d)$ can be represented as: $\sigma(d) = \sigma^{-}(d) + \sigma^{+}(d)$, $S(d) = -\pi^2 k^2 T^2 \dfrac{\sigma^{-}(d) - \sigma^{+}(d)}{e\varepsilon_F \left[\sigma^{-}(d) + \sigma^{+}(d)\right]}$, where ε_F – Fermi energy, k – Boltzmann constant, e – elementary charge. The results of size effect studys of conductivity and thermoelectric power of nanoscale electrically continuous Au and Cu films, showed that electron band structure of films finishes it's formation at about 5 nm Analogous studies of Ni and Pd nanoscale films revealed that with film thicknesses of

4-5 nm and greater, electron structure of layers is identical with electron structure of bulk samples of these metals. It's confirm the completion of electron band formation of *s* – and *d* – bands, which correlates with the experimental results of island metal condensates photoemission studies [43, p. 125; 44, p. 146].

5. Internal mechanical tensiones and self-organization processes on the boundary of "metal condensate – solid substrate"

It is known that on the boundary of "substrate – metal condensate", mechanical tensiones occur balanced by the interaction with the substrate [45, p. 399]. It is believed that total mechanical tension is equal to additive sum of internal (own) σ_i and thermal σ_{TER} tensions: $\sigma = \sigma_i + \sigma_{TER}$. The operational parameters of nanoscale metal films in microelectronics are determined by electrical and mechanical properties. The imbalance of the deposition processes, the difference in the coefficients of thermal expansion of metal condensate and surface substrate, as well as chemical and structural changes cause high mechanical macro and micro tensiones in thin film. The value of internal tensiones can significantly exceed the maximum allowable levels for bulk materials. During the operation of such structures, the relaxation of macro- and micro-tensiones occurs even under minor external loads (thermal heating, charge transfer) and may be accompanied by their destruction or detachment from the substrate. Relaxation of local micro-tensiones leads to the loss of film integrity due to pores formation or material extrusion, which is unacceptable in nanoelectronic elements.

The nature of thermal tension component σ_{TER} has been studied well for many metallic condensates [45, p. 399]. The thermal tension minimization problem is solved today (mostly by technological methods) even in quite complex systems – real structures of modern micro- and nano-electronics. However, the nature of the structural component of mechanical tensiones has not been established. There are only certain model representations of such tensiones mechanisms formation. It's believed that internal tensions are caused by the peculiarities of film formation process, the non-equilibrium of condensation process, recrystallization and interaction of condensates with residual gases [45, p. 399; 46–49]. Understanding the macro- and micro-processes responsible for internal tensions formation will provide the possibility of depositing metal condensates with

improved characteristics for the needs of micro- and nanoelectronics by systematically changing their internal structure and interphase interaction on the boundry "condensate-substrate".

Information about thin films mechanical tensiones which researchers have today, was obtained mostly by indirect methods and after condensates is deposited. Therefore, the results of the measurements carry information only about the integral macrotensiones that occur after the formation of the metal film. However, due to the relaxation of tensiones in the "film – substrate" during its storage, such post-technological measurements do not provide objective information about the quantitative contribution of each component to measured integral value of tensiones and are uninformative from the point of view of learning the physical laws of certain type tensiones formation.

The accumulation of huge experimental material in the field of physics and technology of thin films today made it possible to formulate some empirical regularities (mostly of the technological plan) of the occurrence (formation) of inherent tensiones in thin films [45; 46, p. 18; 50–52]. The determining factor in the analyzed processes is the rate of condensation of metal vapor on substrate surface. However, the mechanisms of formation of grain boundaries in thin films and the physical mechanism of internal tensiones formation based on thermodynamic approach, taking into account changes in surface and interphase energies are currently poorly studied. There is no model of the phenomenon for the initial stage of condensate growth, when it exists in the island-nanodisperse stage. There is no physical vision of mechanisms of maximum tensiones formation in metal condensates depending on the speed of their deposition on the surface substrate. Therefore, the experimental study of regularities of the internal tensiones formation n metal condensates, which reflect the dynamics of interphase interaction from the stage of island-nanodisperse formation to continuous film is an urgent problem of nanoscale materials science.

Among a number of metals tested by modern microelectronics, copper, aluminum and their alloys occupy a key place in the production of micro- and nanoelements on silicon. Moreover, copper significantly expands its position due to its inherent manufacturability, high electrical and thermal conductivity, as well as high resistance to electromigration. The work

experimentally investigated the kinetics of internal tensiones $\sigma_i(d)$ in Cr, Cu, Au and Al metal condensates during their deposition on silicon substrates at room temperature.

The method of measuring the mechanical tensiones that arise in the "film – substrate" system is based on the measurement of the bending of the cantilevered substrate [50–53, p. 24]. The amount of tension that occurs parallel to the plane of the substrate is calculated according to the well-known Stoney formula:

$$\sigma_y = E_s \delta d / (3 d_f l^2 (1 - \mu)) \qquad (12)$$

where E_s – substrate Young's modulus, d – thickness of the substrate; δ – console displacement; d_f – film thickness; l – base of measurements; μ – substrate Poisson's modulus. In this way, the measurement of mechanical tensiones during metal deposition on the substrate is essentially reduced to continuous experimental fixation of its deflection δ. A capacitive method was used for δ registration [53, p. 132].

In Figure 20 shows the experimental dependence which reflect the kinetics of changes in internal tensiones in copper condensates deposited at different rates ω on monocrystalline silicon substrates with the

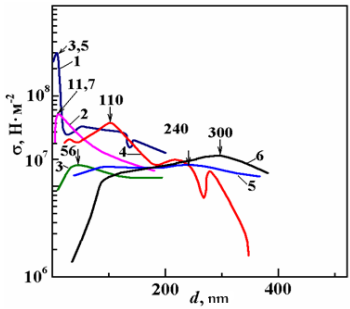

Figure 20. Kinetics of internal (intrinsic) mechanical tensiones in metallic copper condensates on monocrystalline silicon substrates deposited at different velocities ω, nm/s: 1 – 0,03; 2 – 0,09; 3 – 0,2; 4 – 0,5; 5 – 1,0; 6 – 2,0

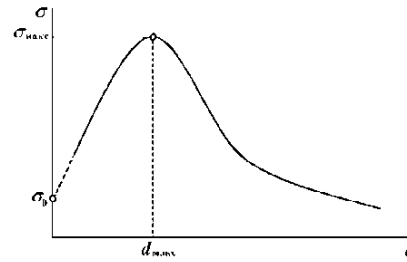

Figure 21. Schematic dependence of the kinetics of internal tensiones of metal condensates on the surface of monocrystalline silicon

crystallographic plane (111) at room temperature. The general regularity of similar dependencies for Cr, Al, and Au films is the two-stage nature of the change in internal tensiones during the formation of vacuum condensates on monocrystalline silicon substrates. There is sharp increase of σ in the first stage of maximum $\sigma_{m\omega}$ at given condensation rate ω and their subsequent decrease with increasing film thickness in the second stage (Figure 21).

The patterns obtained (see Figure 21) are typical for the studied metals. The extrapolation of the first stage of the dependence $\sigma = \sigma(d)$ in the direction of the intersection with the σ axis made it possible to determine the value of the tension σ_0, which corresponds to the characteristic thickness of the nanocondensate $d_0 \approx 10^{-9}$ m (nucleus formation) in relation to the entire range of used condensation rates. In Figure 22 shows $\sigma_0(\omega)$ for Cu, Au, Cr and Al condensates calculated from the experimental size dependences of $\sigma(d)$. As we can see, the constancy of σ_0 within the indicated range of deposition rates and the presence of local maximum of internal tensiones for the listed metals at deposition rate of 0,5 nm/s are characteristic. Al condensates are an exception (Figure 22, curve 1). The analysis of experimental dependences confirms that the positions of the characteristic maxima for a given deposition rate fit on a straight line in the coordinates (Figure 23). Note that, in addition to Cu and Al, the maximum tension coordinates for Cr and Au films are also superimposed on the same line. Therefore, the slope coefficient of this dependence is the same for Cr, Cu, Au, Al. metal condensates on the silicon substrate. Since the parameter $k = \Delta\sigma_{m\omega} / \Delta\omega$, that sets the angular coefficient of the slope of the straight line, in Figure 23 has the dimension of time, then it is logical to assume that it determines the transition time of metal condensates from a highly dispersed (island) structure to a solid film with a spatial frame over the entire area of the substrate at different rates of their deposition in relation to the given crystallographic orientation of the substrate. For the listed metals, this time is ~ 220 s and corresponds to the Ostwald ripening time of the condensate. Stacking the characteristic points of different metals on one line proves the predominant impact of substrate on mechanical tensiones appearance at the initial stage of the Cr, Cu, Au, Al films growth. The obtained conclusion is also confirmed by the date shown in Figure 22, it's demonstrate the invariance of tensiones from the rate of condensation responsible for the formation and growth of nanosized metal islands. Therefore, we can

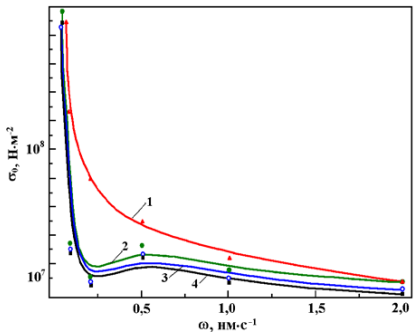

Figure 22. Mechanical tension dependence ($d_0 \approx 10^{-9}$ m) on the condensates rate: Cu (4), Au (3), Cr (2), Al (1)

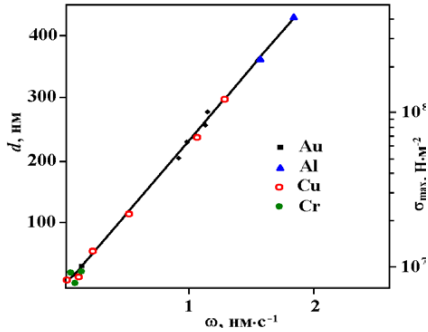

Figure 23. Dependence of the position of the maximum tensiones $\sigma_{m\omega}$ on the experimental dependences of σ(d) by thickness in metal condensates on their deposition rate ω nm/s: 1 – 0,03; 2 – 0,09; 3 – 0,2; 4 – 0,5; 5 – 1,0; 6 – 2,0

state that the occurrence of internal mechanical tensiones in metal nano-condensates of Cu, Au, Al and Cr on the silicon surface is determined by self-organization processes on the surface of silicon substrates. It's provides equivalent conditions for seeds nucleation, growth of crystallization and spreading of non-equilibrium metallic island-dispersed sub-system. We note that the stationary values of the received tensiones σ in thin films after they pass the maximum values during the deposition process are reached often due to relaxation "disruptions" of tensiones at metastable states (Figure 20, curve 4). Several reasons for the observed behavior are assumed: sharp plasticity of the fluidity of the film due to the conservative movement of "fresh" dislocations under the action of internal tensiones; grain-boundary sliding in the film due to the processes of non-conservative movement of "fresh" dislocations, since as a result of supersaturation of the condensate on vacancies ($s \sim 10^{-3}$ [45, p. 146]), local plastic deformation of the condensate occurs. As a result of the effect of the diffusion "dill", there is a "slipping" of individual areas of the film, which is manifested in the sharp bends of the cantilever during the deposition process. The relaxation processes in the "film-substrate" system are also not an exception, due to

the generation of dislocations on the surface of the substrate, since the yield strength of the surface layers of a monocrystalline substrate is significantly lower [54, p. 18]. Implementation of the last of the mechanisms requires its consideration in the development of metal nanocondensate systems in this range of mass thicknesses. Because the mechanical tensiones on the substrate surface it's creates conditions for the defects generation on it. Which significantly reduces the reliability and operational characteristics of nano-sized devices based on them.

Let's analyze the role of the substrate in the formation σ_{max} tensiones of metal condensate (Figure 23). Note that the maximum values σ_{max} for studied metals are observed at the smallest thicknesses in Cr condensates ($\approx$ 50 nm), while in Al films the maximum tension level σ_{max} is achieved at the large thicknesses. Identified regularities in a number of studied metals for σ_{max} can be explained from the standpoint of the adhesive properties of metals on the silicon surface. Therefore, we consider the interaction on the boundary of "metal condensate – silicon" at the atomic level, taking into account the potential ability of the substrate atoms, on the one hand, and the metal condensate, on the other hand, to form chemical bonds. One of the main factors that determines not only the type, but property of bond and the nature of interaction between atoms in chemical reactions, is the electronegativity of the interacting atoms that take part in chemical bonds. Silicon, having a relatively high electronegativity (~ 1,8 according to Pauling [55]), is capable for greater electron attachment than condensed metals (Cr – 1,56; Cu – 1,76; Au – 1,42; Al – 1,47). With such an interaction, the electrons transport to the surface of silicon substrate by metal condensates should be expected. For the studied systems, the value of X_{Si-Me} is always less than 0,4, which, according to [55, p. 298], is accompanied with covalent bond by the partial electrons transport from atoms with lower electronegativity (metals) to atoms with higher electronegativity (Si). The fraction of the ionic component will not exceed ~ 10%. Adhesive properties at the interface of the "silicon – metal condensate" will be determined by such interaction. A decrease in the electronegativity of the metals in the given series (Cr, Cu, Au, Al) in relation to the electronegativity of the substrate should also be accompanied by an increase in the level of intrinsic tensiones at the interface of "substrate-condensate", since the role of the substrate in the bonds creation with adsorbed atoms will increase.

An exception is Cu, among the studied metals, it has an abnormally high value of electronegativity, high diffusion coefficient, great plasticity and the ability to twin and recrystallize even at room temperatures. From this point of view, the described self-organizing processes are those that take place not in the deposited film, as is realized in molecular beam epitaxy of the "semiconductor-semiconductor" type by creating certain spatially periodic structures on the surface of the substrate, but by reconstructing the silicon surface under the influence of the deposited metal with $\Delta X < 0{,}4$. This conclusion is confirmed by the high susceptibility of free silicon surfaces to the observed processes. Currently, about 300 reconstructed silicon surfaces have been discovered [56, p. 45–76]. In the process of metal condensate deposition the reconstructed silicon surface provides the same rheological properties of condensed islands metal and close conditions of thermalization of the molecular beam of deposited metals (Cr, Cu, Au, Al).

Conclusions

1. The process of preparing films of simple (Au, Ag, Cu) and transition (Mn, Hi, Pd and Cr) metals with given average linear grain sizes was controlled, which was achieved by the simultaneous use of "quench deposition" techniques and wetting sublayers (Ge, Sb, Si) with further thermal stabilization in the interval of the first temperature zone of the modified Movchan-Demchyshyn model.

2. Based on the analysis of the dimensional dependences of the resistivity $\rho(d)$ and the absolute differential thermoelectric power $S(d)$ shows that in nanoscale electrically continuous films of Cu and Au, the formation of electronic structure similar to the electronic structure of bulk metal is completed at a thickness of 5 nm.

3. As a result of the first-ever study of the size dependences of kinetic coefficients of continuous nanoscale films of Ni and Pd, the electronic structure identical to electronic structure of bulk metal complets formation of *s*- and *d*-zones at thicknesses greater than 4-5 nm.

4. It was established that the probability of intergranular tunneling of current carriers in the studied metal condensates does not depend on the temperature and thickness of the wetting sublayers (Ge, Sb, Si) and the average linear sizes of crystallites D (at least for 5 nm < D < 28 nm) in the

film, at least for temperature range of 78-300 K, and is determined only by the physical properties of the condensate.

5. It was established that the nature of the interphase interaction in the system "metal condensate (Cu, Al, Cr, Au) – solid substrate (Si)" during the deposition process is synchronously reflected by the kinetic dependences of internal tensiones $\sigma_i(d)$.

6. A feature of the interphase interaction in "metal nanocondensate (Cu, Al, Cr, Au) – solid substrate (Si)" is the dominance of self-organization processes on the surface of the silicon substrate, which provides equivalent conditions for the spreading of a non-equilibrium metallic island-disperse system. The degree of the self-organizing role of the substrate in the formation of nanocondensates is determined by the value of the electronegativity difference of the substrate and condensate materials (for silicon and deposited metals, the condition $\Delta X < 0.4$ is fulfilled, which ensures a stable covalent bond on the boundary of "silicon – metal nanocondensate").

7. The time of maximum level of internal tensiones (Oswald ripening time according to the two-stage dependence) in the process of copper, gold, aluminum, and chromium condensation on Si (111) substrates in the speed range of 0,03–2,0 nm/s is the same (220 s) and is determined by the self-organizing role of the silicon substrate of crystallographic orientation (111).

References:

1. Venables J. (2000). Introduction to Surfaces and Thin Film Processes. *Cambridge U. Press, Cambridge,* 389 p.

2. Kukushkin S. A., Osipov A. V. (1998). Thin-film condensation processes. *Physics-Uspekhi*., vol. 41(10), pp. 983–1014.

3. Barna P. B., Adamik M. (1995). Growth mechanisms of polycrystalline thin films. *Science and Technology of Thin Films*, pp. 1–28.

4. Movchan B. A., Demchishin A. V. (1969). Rost i struktura tonkich tverdotelnych plenok. *Phys. Met. Metallogr*., vol. 28, pp. 83–91.

5. Ekinci K. L., Valles J. M. (1998). Thickness dependence of the morphology of ultrathin quench condensed gold films. *Physical Review B*., vol. 58(11), pp. 7347–7350.

6. Movchan B., Demchishin A.V. (1969). Study of the structure and properties of thick vacuum condesates of nickel, titanium, tungsten, aluminum oxide and zirconium oxide. *Phys. Met. Metalogr.,* vol. 28, pp. 653–662.

7. Smilauer P. (1991). Thin metal films and percolation theory. *Contempopary Physics*, vol. 32(2), pp. 89–102.

8. Fuchs K. (1938). The conductivity of thin metallic films according to the electron theory of metals. *Proc. Cambridge Philos. Soc*., vol. 34(1), pp. 100–108.

9. MacDonald D. K. C., Sarginson K. (1950). Size effect variation of the electrical conductivity of metals. *Proc. R. Soc. Lond. A*., vol. 203, pp. 223–240.

10. Stasyuk Z. V., Lopatinsky A. I. (2001). Size-Dependent Kinetic Phenomena in Thin Metal Films. Classic Effects (review). *Physics and Chemistry of Solid State*, vol. 2(4), pp. 521–541.

11. Lucas M. S. R. (1964). Surface scattering of conduction electrons in gold films. *Appl. Phys. Lettv*., vol. 4, pp. 73–76.

12. Lucas M. S. R. (1965). Electrical conductivity of thin metallic films with unlike Surfaces. *J.Appl. Phys*., vol. 36(5), pp. 1632–1635.

13. Greene R. F., O'Donnel R. W. (1966). Scattering of conduction electrons by localized surface charges. *Phys. Rev*., vol. 147, pp. 599–602.

14. Greiner A., Vecchi M. C., Rudan M. (1998). Modelling surface-scattering effects in the solution of the Boltzmann transport equation based on the spherical-harmonics expansion. *Semiconductor Science and Technology*, vol. 13(10), pp. 1080–1089.

15. Ziman J. M. (2001). Electrons and Phonons. The Theory of Transport Phenomena in Solids. Oxford Classic Texts in the Physical Sciences. 567 p.

16. Cottey A. A. (1967). The electrical conductivity of thin metal films with very smooth surfaces. *Thin Solid Films*, vol. 1(4), pp. 297–307.

17. Soffer S. B. (1967). Statistical model for the size effect in electrical conduction. *J.Appl.Phys*., vol. 38(4), pp. 1710–1715.

18. Soffer S. B. (1970). Effect of weak surface autocorrelation on the size effect in electrical conduction. *Phys.Rev.B.: Solid State*, vol. 2, pp. 3894–3899.

19. Mayadas A. F., Shatzkes M., Janak J. F. (1969). Electrical resistivity model for polycrystalline films: the case of specular reflection at external surfaces. *Appl. Phys. Letters*, vol. 14, pp. 345–350.

20. Mayadas A. F., Shatzkes M. (1970). Electrical resistivity model for polycrystalline films: the case of arbitrary reflection at external surfaces. *Phys. Rev. B.: Solid State*, vol. b4, pp. 1382–1389.

21. Tellier C. R., Tosser A. J. (1977). Size effects in thin solid films. Amsterdam: Elsevier publ. Co., p. 310.

22. Pichard C. R., Tellier C. R., Tosser A. J. (1979). A three-dimensional model for grain boundary resistivity in metal films. *Thin Solid Films*, vol. 62(2), pp. 189–194.

23. Pichard C. R., Tellier C. R., Tosser A. J. (1981). Empirical result establishing the thermal independence of the grain boundary reflection coefficient. *Electrocomp. Sci. and Technology*., vol. 7(7), pp. 217–220.

24. Pichard C. R., Bedda M., Bouhala Z., Quarbya L., Tosser A. J. (1985). Energy dependence of the theoretical expressions of Ziman transport parameters in the Mayadas-Shatzkes model. *Journ. Mat. Sci*., vol. 20(3), pp. 867–872.

25. Deschacht D., Boyer A. (1985). General expression for the temperature coefficient of resistivity of polycrystalline semi-metal films. *J. of Matterials Science*, vol. 20(3), pp. 807–811.

26. Pichard C. R., Tellier C. R., Quarbya L., Tosser A. J. (1982). Effect de grains non cubiques sur la conductivite electrique de coeches metalliques polycrystallines. *Le Vide, les Couches Minces*., vol. 210(1-2), pp. 3–12.

27. Bedda M., Pichard C. R., Tosser A. J. (1986). Numerical approximations for transport parameters in the framework of multidimensional conduction models. *Journ. Mat. Sci*., vol. 21, pp. 1405–1412.

28. Tijani H., Pichard C. R., Tosser A. J. (1987). Isotropy of the grain boundary scattering in the framework of a multidimensional conduction model. *Journ. Mat. Sci*., vol. 6(9), pp. 1107–1109.

29. Tosser A. J., Pichard C. R., Lahrichi M., Bedda M. (1985). Simple calculation of the Hall coefficient of thin metal films. *Journ. Mat. Sci. Lett*., vol. 4(5), pp. 585–588.

30. Tellier C. R., Tosser A. J., Boutrit C. (1977). The Mayadas-Shatzkes conduction model treated as a Fuchs-Sondheimer model. *Thin Solid Films*, vol. 44, pp. 201–208.

31. Ukhlinov G. A., Kossakovskaya Z. Ya. (1983). Electrical conductivity of polycrystalline metal samples with shape-size structure. *Physics of Metals and Metallography*, vol. 55(1), pp. 61–64.

32. Namba Y. (1970). Resistivity and its temperature coefficient of thin metal films with rough surface. *Jap. J. Appl. Phys.*, vol. 9, pp. 1326–1329.

33. Abrosimov A. M., Egorov B. N., Lydorenko N. S. (1974). Razmernyy effekt koeffitsiyentov perenosa v teksturirovanykh plenkakh vismuta, vyrashchennykh na polimernykh podlozhkakh [Size effect of transfer coefficients in textured bismuth films grown on polymer substrates]. *Teplofizika vysokikh temperatur – Thermophysics of high temperature*s, vol. 17(3), pp. 531–536.

34. Finzel H. U., Wissman P. (1986). The d^{-3} law describing the thickness dependence of the electrical resistivity of rough metal films. *Annalen der Physik*. Folge 7, Band 43, Heft 1/2. S. 5–10.

35. Wissmann P., Finzel H. U. (2007). Electrical Resistivity of Thin Metal Films. *Springer Tracts in Modern Physics*, vol. 223, p. 128.

36. Smilauer P. (1991) Thin metal films and percolation theory. *Contemporary Physics*, vol. 32(2), pp. 89–102.

37. Bihun R. I., Stasyuk Z. V. (2014). Impact of Surface Inhomogeneities on Charge Transport in Ultrathin Metals Films. *Metallofiz. Noveishie Tekhnol*, vol. 36(6), pp. 723–734. (in Ukrainian)

38. Bihun R. I., Buchkovska M. D., Gavrilyukh V. M., Kravchenko O. E., Stasyuk Z. V., Leonov D. S. (2014). The Formation of Metallic Electrical Conduction in Vacuum Condensates Metals Films. *Metallofiz. Noveishie Tekhnol*, vol. 36(4), pp. 531–546. (in Ukrainian)

39. Bihun R. I., Kravchenko O. E., Leonov D. S. Pastirskiy Ya. A. (2013). The effect of germanium underlayers of subatomic thickness on the structure and low-temperature thermo-e.r.s. of gold and copper ultra-thin films. *Metallofiz. Noveishie Tekhnol*, vol. 35(5), pp. 603–609. (in Ukrainian)

40. Shpak A. P., Bihun R. I., Stasyuk Z. V., Kunitsky Yu. A. (2010). Structure and Electroconductivity of Ultrathin Films of Copper, Gold and Silver. *Наносистеми, наноматеріали, нанотехнгології,* vol. 8(2), pp. 339–388. (in Ukrainian)

41. Melnychuk B. L., Lopatynskyi A. I., Stasyuk Z. V. (1998). Electrical conductivity and thermo-e.p.f of thin palladium, nickel and molybdenum films. *Фізичний збірник НТШ*, vol. 3, pp. 124–132.

42. Panchenko O. A., Luchshun P. P., Ptushinsky U. H. (1969). Galvanomagnetic phenomena in thin films of some transition metals. *JETP*, vol. 56(1), pp. 134–138.

43. Katrich G. A., Naumovets A. G. (1988). Photoelectron spectroscopy of small particles and thin films of s- and d-metals: size effect in their electron structure. *Studies in Surface Science and Catalysis*, vol. 40, pp. 123–130.

44. Fedorovich R. D., Naumovets A. G., Tomchuk P. M. (1999). Hot electrons in nanoparticles: A model of electron and light emission from island metal films. Physics, chemistry and application of nanostructures. *Reviews and short notes to nanomeeting*, pp. 145–147.

45. Venables J. A., Spiller G. D. T., Hanbucken M. (1984). Nucleation and growth of thin films. *Reports on Progress in Physics*, vol. 47(4), pp. 399.

46. Kukushkin S. A. (1994). Evolution processes in multicomponent and multiphase film growth from solutions. *Thin Solid Films*, vol. 239(1), pp. 16–26.

47. Laugier M. (1981). Adgesion and internal tension in thin films of aluminium. *Thin Solid Films*., vol. 79 (1), pp. 15–20.

48. Janda M. Stefan O. (1984). Intrinsic in chromium thin films measured by a Novel method. *Thin Solid Films*, vol. 112(2), pp. 127–137.

49. Laugier M. (1981). The effect on ion bombardment on tension and adhesion in thin films of silver and aluminium. *Thin Solid Films*, vol. 81(1), pp. 61–69.

50. Spaepen F. (2000). Interfaces and tensiones in thin films. *Acta Materialia*, vol. 48(1), pp. 31–42.

51. Nix W. D. (1989). Mechanical properties of thin films. *Met. Trans*. A., vol. 20A, pp. 2217–2245.

52. Flinn P. A. (1995). Mechanical tensiones in VLSI interconnections: origins, effects, measurement and modeling. *MRS Bulletin*, vol. 20(11), pp. 70–73.

53. Maissel L. I., Glang R., Budenstein P. P. (1970). Handbook of Thin Film Technology. *Technology & Engineering*, vol. 118(4), 1194 p.

53. Handbook of Thin Metal Film Technology (Part I). Edited by Leon I. Maissel and Reinhard Glang. McGRAW Hill Hook Company. 1970. 664 p.

54. Jian Wang, Qing Zhou, Shuai Shao, Amit Misra (2017). Strength and plasticity of nanolaminated materials. *Materials Research Letters*, vol 5(1), pp. 1–20.

55. Pauling L. (1984). The Metallic orbital and the nature of metals. *Journal of Solid State Chemistry*, vol. 54, pp. 297–307.

56. Koman B. P. (2017). Patterns of interphase interaction in near-surface layers of solid-state electronics structures: monograph. Lviv, 350 p.